https://doi.org/10.5194/wes-2020-11
Preprint. Discussion started: 12 February 2020

Characterisation of the Offshore Precipitation Environment to Help Combat Leading Edge Erosion of Wind Turbine Blades

Robbie Herring[1], Kirsten Dyer[1], Paul Howkins[1], Carwyn Ward[2]

[1]Offshore Renewable Energy Catapult, Offshore House, Albert Street, Blyth, NE24 1LZ, UK
[2]Department of Aerospace Engineering, Queen's Building, University of Bristol, Bristol, BS8 1TR, UK

Correspondence to: Robbie Herring (robbie.herring@ore.catapult.org.uk)

Abstract. Greater blade lengths and higher tip speeds, coupled with a harsh environment, has caused blade leading edge erosion to develop into a significant problem for the offshore wind industry. Current protection systems do not last the lifetime of the turbine and require regular replacement. It is important to understand the characteristics of the offshore environment to model and predict leading edge erosion. The offshore precipitation environment has been characterised using up to date measuring techniques. Heavy and violent rain was rare and is unlikely to be the sole driver of leading edge erosion. The dataset was compared to the most widely used droplet size distribution. It was found that this distribution did not fit the offshore data and that any lifetime predictions made using it are likely to be inaccurate. A general offshore droplet size distribution has been presented that can be used to improve lifetime predictions and reduce lost power production and unexpected turbine downtime.

1 Introduction

The offshore wind industry's need of larger rotors and higher tip speeds has caused blade leading edge erosion to develop into a major problem for the industry. Leading edge erosion is caused by raindrops, hailstone, and other particles impacting the leading edge of the blade and removing material. This degrades the aerodynamic performance of the blade and requires operators to perform expensive repairs. The issue has grown in prominence recently with reports that Ørsted had to make repairs to up to 2,000 offshore wind turbines after just a few years of operation (Finans, 2018).

The industry attempts to prevent the onset of leading edge erosion by applying protection systems, such as coating and tapes, to the blade leading edge. However, currently these do not last the lifetime of the turbine and require regular replacement.

Several analytical models that aim to estimate the expected lifetime of a protection system have been developed (Eisenberg et al., 2018, Slot et al., 2015, Springer et al., 1974). Finite element models that can predict the stresses and strains in a protection system from an impinging water droplet have also been produced (Keegan et al., 2012, Doagou-Rad and Mishnaevsky, 2019). To model leading edge erosion, it is important to understand the characteristics of the impinging hydrometeors and, as rain is the most frequent hydrometeor, the droplet size distribution (DSD) of the impinging rain.

https://doi.org/10.5194/wes-2020-11
Preprint. Discussion started: 12 February 2020

Weather radars are widely used to predict the offshore precipitation environment due to their ability to examine large geographical areas. To translate the radar data to DSDs, it is passed through complex algorithms and, due to the lack of offshore rain datasets, validated against onshore datasets collected from strain gauges and disdrometers. The most extensively used onshore distribution is the Best distribution published in 1950 (Best, 1950). However, the manual measurement techniques used by Best are outdated and have been found to provide inaccurate results (Kathiravelu et al., 2016).

The lack of an offshore dataset introduces uncertainty into radar predictions and, as a result, validation inaccuracies may exist. In this work, state of the art measurement techniques have been used to characterise the offshore precipitation environment and provide the required offshore dataset. A general offshore DSD is also presented.

2 The Best Distribution

The most widely used DSD is the Best distribution. Best takes the work of several authors and converts them into a common DSD defined as:

$$1 - F = exp\left[-\left(\frac{x}{a}\right)^{n}\right], \quad (1)$$

where F is fraction of liquid water in the air comprised by drops with diameter less than x, I is the rate of precipitation and

$$a = AI^{p}, \quad (2)$$

where $A = 1.30, p = 0.232, n = 2.25$. Best concluded that the constant n is independent of the precipitation intensity. This is commonly presented in literature as:

$$F(x) = 1 - exp\left[-\left(\frac{x}{1.3\ I^{0.232}}\right)^{2.25}\right], \quad (3)$$

Data was predominantly collected by two manual methods; the 'Stain' method and the 'Flour Pellet' method. In the Stain method, a sheet of absorbent paper is exposed to the rain for a short time. The stains made by the droplets are rendered permanent by previously treating the paper with a suitable powder dye. Then, the stains are counted, measured and interpreted in terms of drop sizes. A calibration curve specific to the filter paper is used to relate the stain diameter to the droplet diameter. The spread factor relationship is dependent upon the physical properties of the fluid, drying conditions and the impact velocity of the droplet (Sommerville and Matta, 1990). In the Flour Pellet method, rain is allowed to fall into pans of silted flour. The resulting dough pellets are baked and subsequently sized by passing them through graded sieves.

In both measurement techniques, sampling can only occur in short intervals. Best performs measurements using the Stain method for a maximum of two minutes. During prolonged periods of sampling, the droplet stains and pellets can overlap, making it difficult to accurately measure and count individual drops. Furthermore, the techniques also have a low resolution.

https://doi.org/10.5194/wes-2020-11
Preprint. Discussion started: 12 February 2020

Best registers droplet sizes in 0.5 mm intervals. Given that the distribution predicts that for a rain rate of 1 mm/hr, most droplets are between 0 and 2 mm, it is clear that a higher resolution is required for effective analysis.

3 Offshore Measurement Technique

Two Campbell Scientific PWS100 disdrometers have been installed onto Offshore Renewable Energy Catapult's offshore anemometry hub, which is located three nautical miles from the coast of Blyth, Northumberland. Fig. 1 shows the position of the two disdrometers, with the first mounted on the existing platform 25 m metres above sea level and the second mounted 55 m above sea level.

Figure 1: The optical disdrometers mounted to the platform (left) and at 55 m above sea level (right).

The optical disdrometers are non-intrusive and do not influence drop behaviour during measurement. They have also been shown to successfully resolve droplet break-up and splatter problems experienced by other measurement techniques (Kathiravelu et al., 2016). Agnew (Agnew, 2013) found that the PWS100 slightly underestimates the number of droplets with a diameter below 0.8 mm. However, the measurement of larger, more damaging droplets was found to be accurate.
DSD data from 1st September 2018 up to and including the 31st August 2019 is presented to provide a 12 month period for analysis. This allows analysis to also be completed seasonally. Hydrometeors have been recorded with a resolution of 0.1 mm. Data is available with a time interval of 1 minute.

Table 1 presents the percentage of available data for each month and the percentage of the available data in which precipitation was recorded. An estimation of the actual percentage of precipitation can be obtained by assuming that the same proportion of precipitation occurred across the unavailable data. A total of 82.89% of the data was available during the

https://doi.org/10.5194/wes-2020-11
Preprint. Discussion started: 12 February 2020

entire measurement period. Precipitation was recorded in 8.71% of the available data giving a yearly precipitation estimate of 10.50%. Winter had the highest estimation of total time with precipitation with 12.07%, whilst spring saw the lowest with an estimation of 8.65%.

Table 1: Percentage of available data for each month.

Month	Percentage of available values (%)	Percentage of time with precipitation (%)	Estimation of total time with precipitation (%)
September 2018	88.84	5.81	6.54
October 2018	98.55	8.57	8.70
November 2018	96.29	10.30	10.70
December 2018	90.11	9.73	10.80
January 2019	81.42	10.69	13.13
February 2019	68.43	7.35	10.74
March 2019	75.94	7.82	10.30
April 2019	91.24	4.83	5.29
May 2019	72.50	11.19	15.43
June 2019	83.28	13.31	15.98
July 2019	53.43	5.53	10.35
August 2019	94.66	9.35	9.88
Total	82.89	8.71	10.50

4 The Offshore Dataset

In line with recommendations from Chen (Chen et al., 2016) and Vejen (Vejen et al., 2018), quality control was performed on the raw data collected from the disdrometers. Data was neglected if it met any of the following criteria:

- Event had a duration of 1 minute or under,
- Event had less than 10 hydrometeors recorded in total,
- Events where the disdrometer recorded a rain rate of 0, but hydrometeors were recorded.

4.1 Precipitation Intensity Frequency

The average precipitation intensity was recorded every minute. Fig. 2 presents its variation across the measurement period, and Fig. 3 presents the cumulative frequency of the recorded intensities. The median precipitation intensity for the measurement period was 0.311 mm/hr.

Precipitation is classified according to its intensity with the following categories defined by the Met Office (Met Office, 2007):

- Light – precipitation intensity less than 2.5 mm/hr,
- Moderate – precipitation intensity between 2.5 mm/hr and 10 mm/hr,
- Heavy – precipitation intensity between 10 mm/hr and 50 mm/hr,

https://doi.org/10.5194/wes-2020-11
Preprint. Discussion started: 12 February 2020

- Violent – precipitation intensity greater than 50 mm/hr.

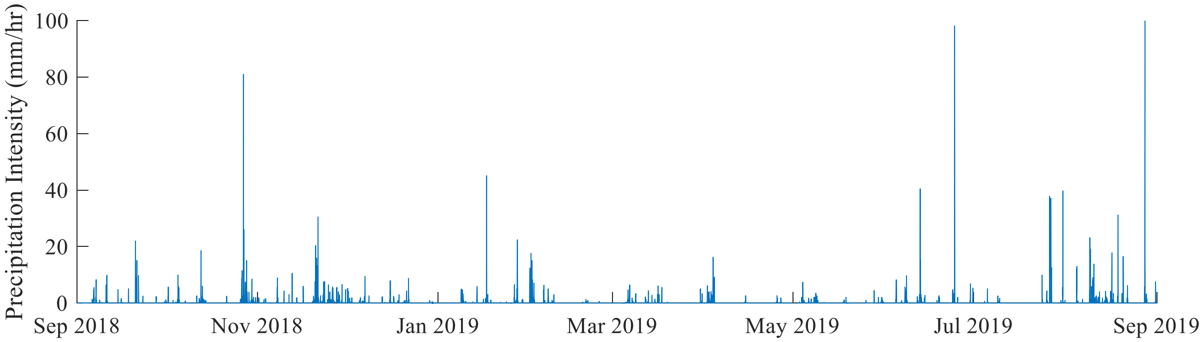

Figure 2: Precipitation intensity during the measurement period.

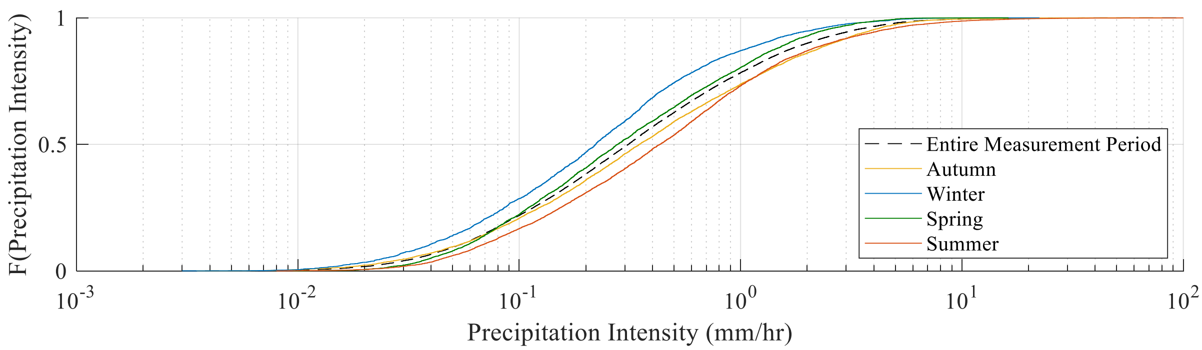

Figure 3: Cumulative distribution of precipitation for the respective seasons.

Table 2: Precipitation intensity distribution for seasons and intensity categories.

	Median precipitation intensity (mm/hr)	Percentage of precipitation category (%)			
		Light	Moderate	Heavy	Violent
Autumn	0.3492	89.42	10.09	0.46	0.03
Winter	0.2217	96.43	3.49	0.08	0
Spring	0.2778	98.56	1.44	0	0
Summer	0.4321	89.87	8.85	1.16	0.12
Total	0.3111	92.58	6.89	0.50	0.03

The seasonal breakdown of precipitation categories is shown in Table 2. Summer had the highest median precipitation intensity with the highest amount of recorded heavy and violent precipitation. In contrast, winter and spring saw minimal heavy precipitation and no violent precipitation. Light precipitation dominated across the entire measurement period accounting for 92.58% of all precipitation. Furthermore, 78.31% of the recorded minutes had an intensity lower than 1 mm/hr. Moderate precipitation was recorded in 6.89% of all cases, whilst heavy and violent rain occurred in 0.50% and 0.03% cases, respectively. This corresponds to a total of 151 minutes of heavy precipitation and only 9 minutes of violent

https://doi.org/10.5194/wes-2020-11
Preprint. Discussion started: 12 February 2020

precipitation across the year. This gives a total of 193 minutes a year of heavy and violent rain once the unavailable data is factored in.

Therefore, a wind turbine in this location would experience less than 3.5 hours a year of precipitation with an intensity greater than 10 mm/hr. Without corresponding erosion data, it is not possible to conclude if erosion damage is predominantly caused by heavy and violent precipitation. However, given that erosion can occur within just a few years of installation and assuming that heavy and violent precipitation occurs with the same frequency as found in this dataset, a turbine would experience less than a day of high intensity rain before erosion occurs. This suggests that erosion damage is not driven solely by heavy and violent precipitation disagreeing with current research theories (Bech et al., 2018).

4.2 Hydrometeor Frequency

Fig. 4 presents the number of recorded hydrometeors by type during the data collection period. The hydrometeor type is clearly dominated by rain droplets. 'Errors' and 'unknown' particles accounted for 17.93% of all data recorded. These may be caused by insects, particles between states or equipment failures and have been neglected. Drizzle and rain droplets make up a combined 98.45% of all hydrometeors recorded. The number of ice pellets, hail and graupel particles recorded was low, accounting for only 0.49% of hydrometeors recorded.

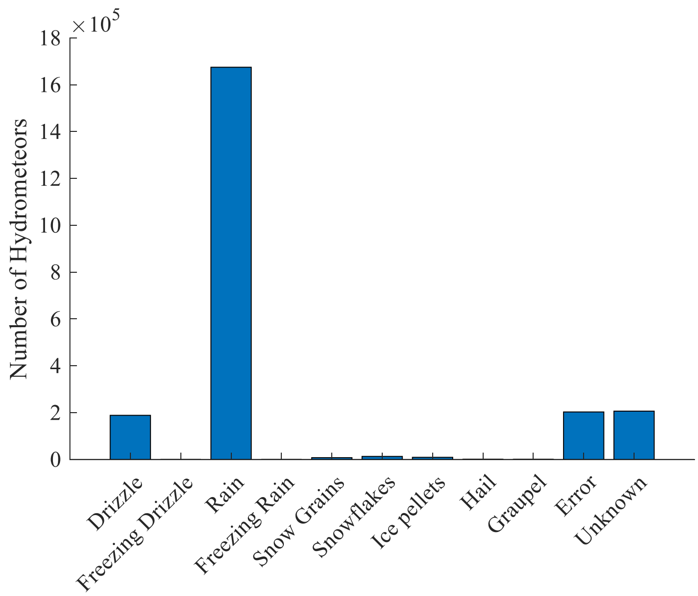

Figure 4: Number and type of hydrometeors recorded during the total measurement period.

As expected, ice and snow based hydrometeors occurred most frequently in winter. Ice pellets, hail and graupel accounted for 0.94% of the hydrometeors recorded in the season with snow grains and snowflakes accounting for 3.56%. In contrast, only 0.16% of hydrometeors recorded in summer were ice pellets or hail, with no graupel, snow grains or snowflakes. Spring and autumn respectively recorded 0.31% and 0.57% of ice pellets, hail and graupel.

https://doi.org/10.5194/wes-2020-11
Preprint. Discussion started: 12 February 2020

4.3 Hydrometeor Velocity

The severity of a hydrometeor impact is governed by its kinetic energy. Whilst the blade speed provides most of the impact velocity, the hydrometeor fall velocity and mass are important. For each minute, the average diameter and velocity was plotted for the modal hydrometeor type. This is presented in Fig. 5.

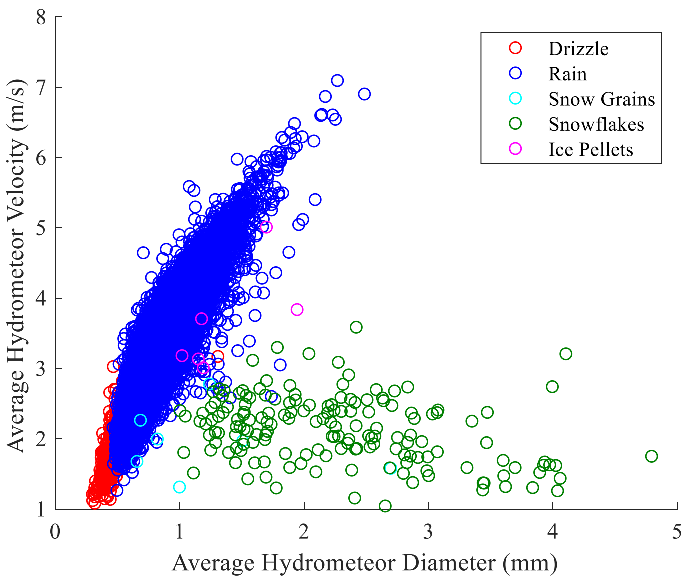

Figure 5: Relationship between size and velocity for the modal hydrometeor at each minute.

There is a clear distinction between water particles and snow particles, with snow particles occurring across a wider range of diameters and lower velocities than rain particles. For the few cases where ice pellets were the model hydrometeors, they all occurred to the right of the rain droplet scatter, indicating that they have a lower fall velocity that rain droplets. There were no cases where hail or graupel were the modal hydrometeor and they were found to be mixed in with rain particles.

5 Offshore Rain Distribution

To accurately translate weather radars into DSDs and reduce uncertainties in radar predictions, a general equation for an offshore DSD is required. The Best DSD has been reproduced, both seasonally and non-seasonally, with updated constants for the offshore rain data presented. Only data where rain particles were the modal hydrometeor were examined.

5.1 Constant Derivation

For each recorded minute, the cumulative function, F, has been evaluated.

Rearranging Eq. (1) gives:

https://doi.org/10.5194/wes-2020-11
Preprint. Discussion started: 12 February 2020

$$\ln \ln\left(\frac{1}{1-F}\right) = n \ln x - n \ln a\ , \tag{4}$$

Values of n and a for the average precipitation intensity over the minute can therefore be determined by plotting Eq. (4). Fig. 6 presents the evaluation of Eq. (4) across a range of precipitation intensities.

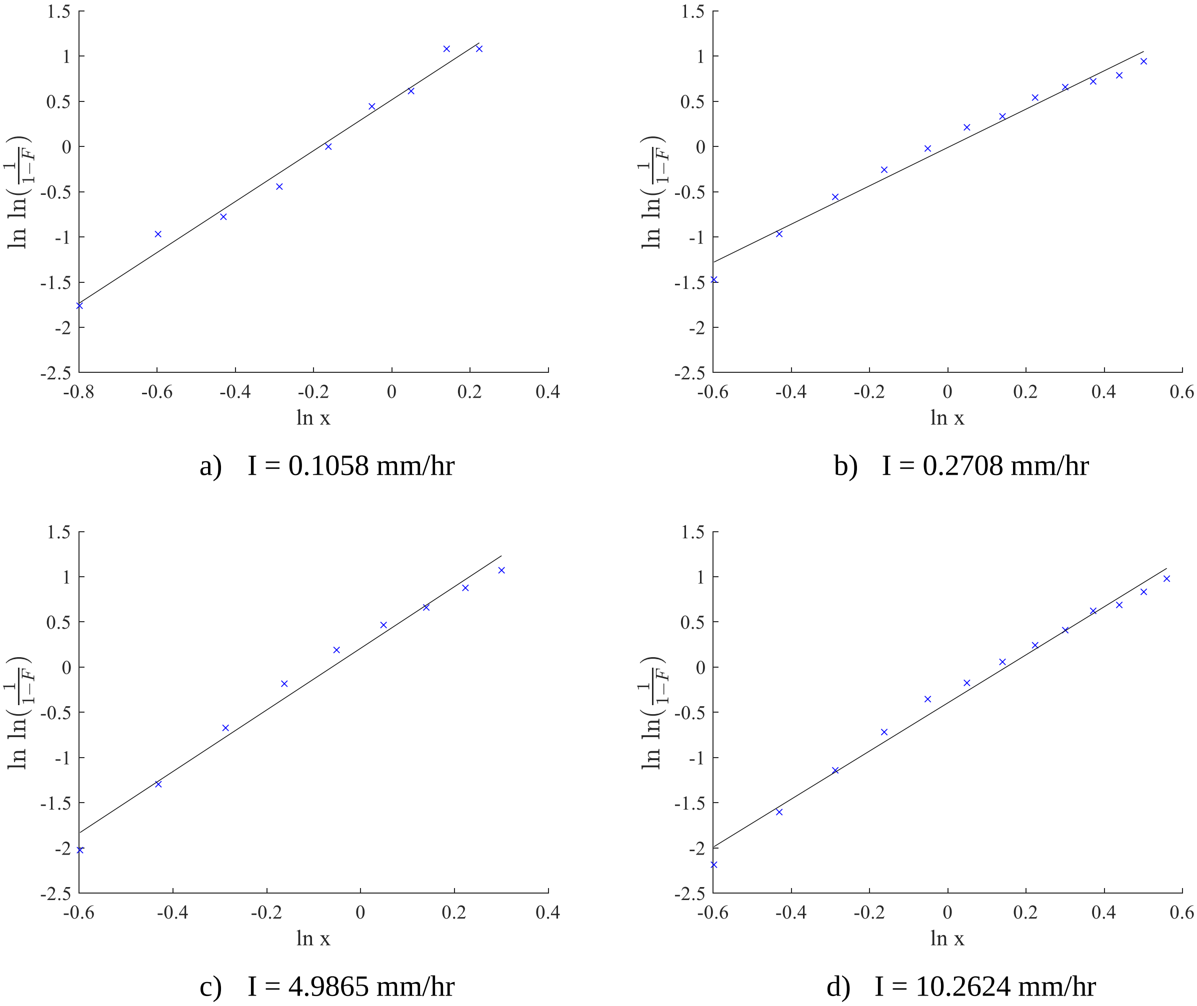

Figure 6: Evaluation of Eq. (4) for precipitation intensities a) 0.1058, b) 1.2708, c) 4.9865 and d) 10.2624 mm/hr.

Rearranging Eq. (2) gives:

$$\ln a = p \ln I + \ln A\ , \tag{5}$$

By plotting Eq. (5), the constants A and p can be obtained. Fig. 7 evaluates Eq. (5) across the whole dataset.

https://doi.org/10.5194/wes-2020-11
Preprint. Discussion started: 12 February 2020

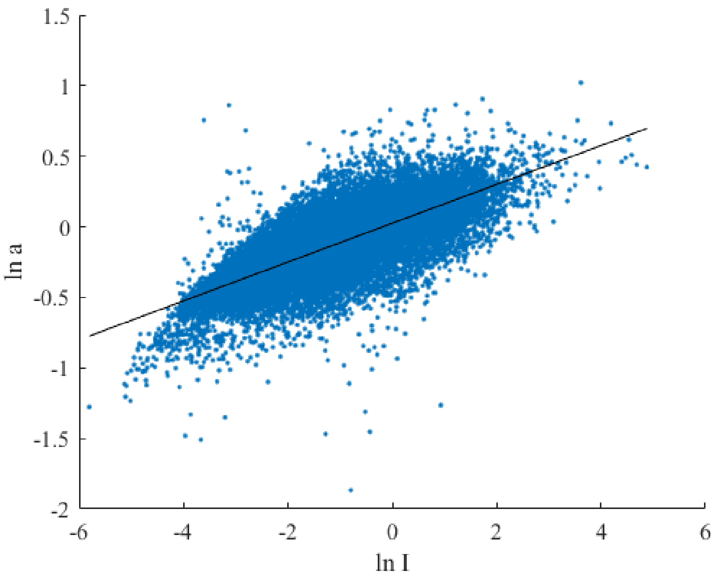

Figure 7: Evaluation of Eq. (5) to derive the constants A and p.

The constants A and p are determined as 1.0260 and 0.1376, respectively.

Best concluded that the constant n is independent of the precipitation intensity. However, for the data presented, n has dependence on the rain rate. The following relationship applies:

$$n = NI^q \, , \tag{6}$$

This can be evaluated as:

$$\ln n = q \ln I + \ln N \, , \tag{7}$$

Fig. 8 presents the plot of Eq. (7) from which the constants N and q can be obtained.

https://doi.org/10.5194/wes-2020-11
Preprint. Discussion started: 12 February 2020

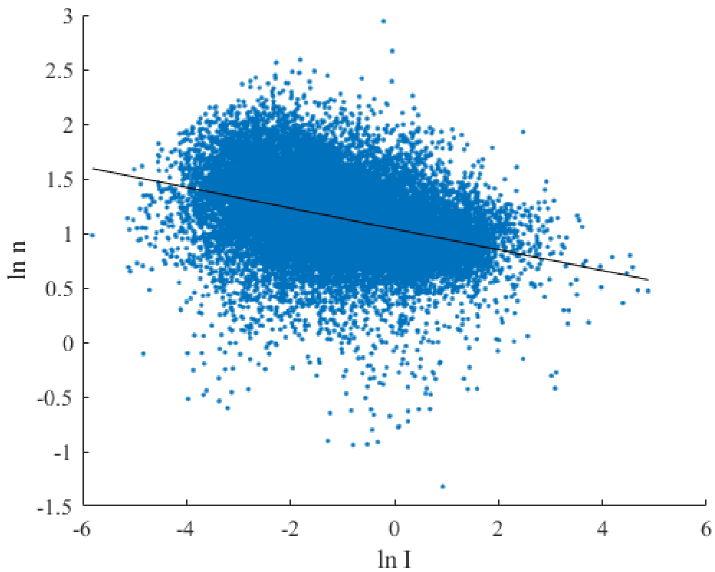

Figure 8: Evaluation of Eq. (7) to derive the constants N and q.

The constants N and q are determined as 2.8264 and -0.0953, respectively. Fig. 8 shows substantial scatter in determining these constants. However, as q is small there is only slight dependence of n on the precipitation rate and whilst the scatter is likely to introduce some error, it does not have a significant effect on the resulting DSD. Table 3 summarises the constants for the non-seasonal distribution.

Table 3: Determined constants for the non-seasonal offshore DSD.

Constant	Value
A	1.0260
p	0.1376
N	2.8264
q	-0.0953

Reproducing Eq. (1) with the derived constants gives a general non-seasonal offshore DSD:

$$F(x) = 1 - exp\left[-\left(\frac{x}{1.03\ I^{0.138}}\right)^{\frac{2.83}{I^{0.0953}}}\right], \quad (8)$$

This is presented for various precipitation intensities in Fig. 9. Table 4 presents the constants for seasonal DSDs. For detailed modelling and lifetime predictions it may be favourable to use season dependent DSDs.

https://doi.org/10.5194/wes-2020-11
Preprint. Discussion started: 12 February 2020

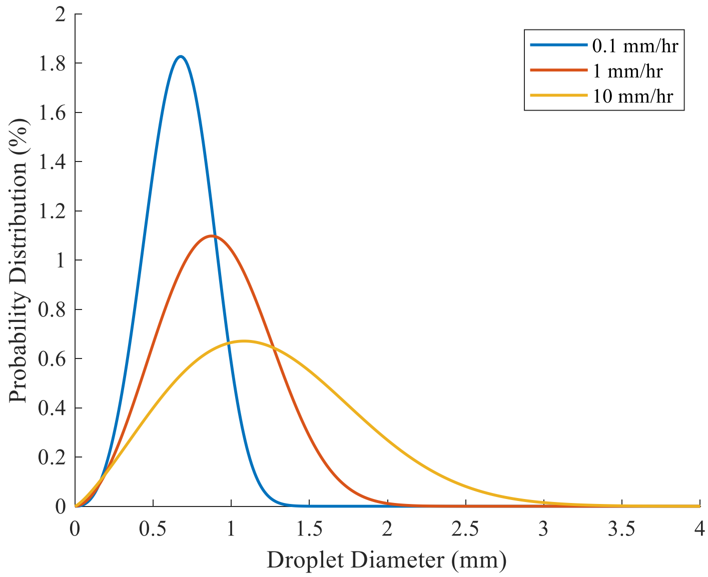

Figure 9: The non-seasonal offshore DSD at different precipitation intensities.

175 **Table 4: Determined constants for the seasonal offshore DSDs.**

Season	Data used (%)	*A*	*p*	*N*	*q*
Autumn	27.62	0.9723	0.1335	2.7762	-0.0911
Winter	24.95	0.9831	0.1338	2.6581	-0.1136
Spring	20.43	1.0393	0.1270	2.8282	-0.1065
Summer	27.00	1.0937	0.1410	2.9657	-0.0893

5.2 Sensitivity Analysis

The sensitivity of the constants to the data selected has been evaluated. The following cases have been examined:

- Low and high precipitation intensity have been individually and collectedly neglected. Precipitation intensities below 0.1 mm/hr and above 10 mm/hr were neglected.
- Precipitation intensities that account for a small number of the recorded intensities have been individually and collectively neglected. These are the bottom 1% and the top 1%.

Minutes where the measured precipitation intensity is low generally record fewer droplets than those with higher precipitations. Conversely, a significant number of droplets are generally seen in heavy precipitation. Low and heavy intensity rain may, therefore, have a high scatter that could influence the determined constants. Fig. 3 presented the cumulative distribution of the recorded precipitation intensities. The bottom and top 1% of precipitation intensities may also skew the data by providing a point significantly different to the trend. The impact of these conditions on the constants is shown in Table 5.

https://doi.org/10.5194/wes-2020-11
Preprint. Discussion started: 12 February 2020

Table 5: Sensitivity of constants to the selected cases.

Precipitation Intensities (mm/hr)	Data Used (%)	*A*	*p*	*N*	*q*
I	100	1.0260	0.1376	2.8264	-0.0953
I > 0.1	77.68	1.0218	0.1249	2.8132	-0.1067
I < 10	96.85	1.0269	0.1382	2.8227	-0.0961
0.1 < I < 10	6.89	1.0219	0.1252	2.8071	-0.1090
I > 0.0158	99	1.0245	0.1350	2.8223	-0.0979
I < 6.95	99	1.0280	0.1388	2.8192	-0.0969
0.0158 < I < 6.95	98	1.0263	0.1360	2.8144	-0.0997

In general, the constants are consistent across all the examined cases. The constant p is the most sensitive to the data included. Neglecting low precipitation intensities reduces its value, whilst neglecting higher intensities increases its value. Removing precipitation intensities below 0.1 mm/hr has the greatest effect on the constants. However, ignoring these intensities loses 22.32% of the data available. It can be concluded that the proposed constants are acceptable.

5.3 Comparison to Best DSD

The general offshore DSD has been compared to the Best DSD at various precipitation intensities in Fig.10. The precipitation intensities 0.1, 1, 2.5, 5, 10, 20 mm/hr were selected to enable comparison of the two DSDs across a range of intensities. To account for variability in the recorded results, minutes which recorded an intensity within ±5% of the selected intensity were included. For each data group, the intensities were averaged and the offshore DSD and Best DSD for the average intensity plotted against them.

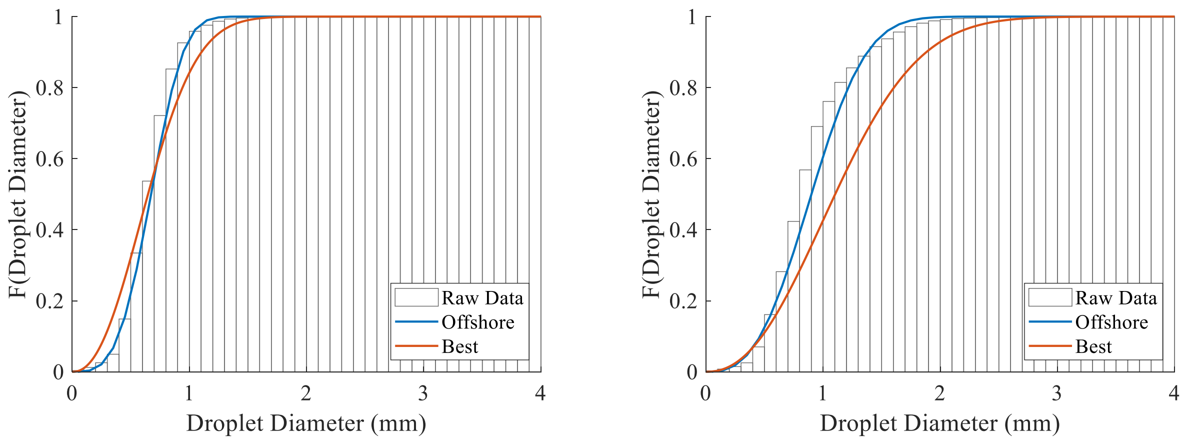

a) I = 0.10005 mm/hr

b) I = 0.99612 mm/hr

https://doi.org/10.5194/wes-2020-11
Preprint. Discussion started: 12 February 2020

eawe european academy of wind energy
Open Access WIND ENERGY SCIENCE DISCUSSIONS

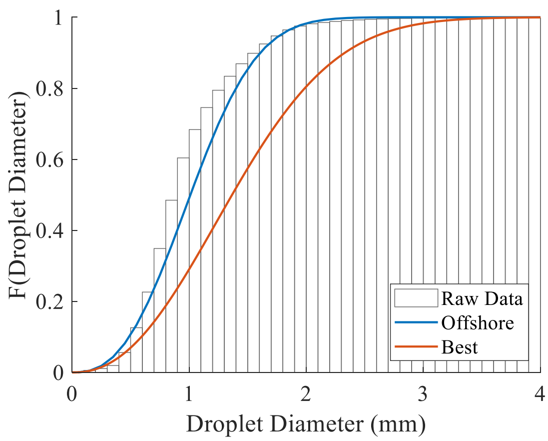

c) I = 2.501 mm/hr

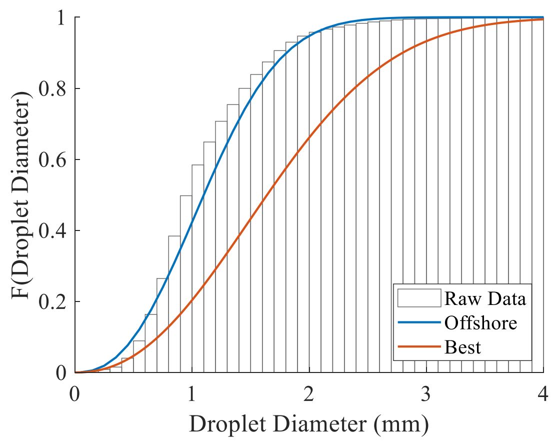

d) I = 4.9818 mm/hr

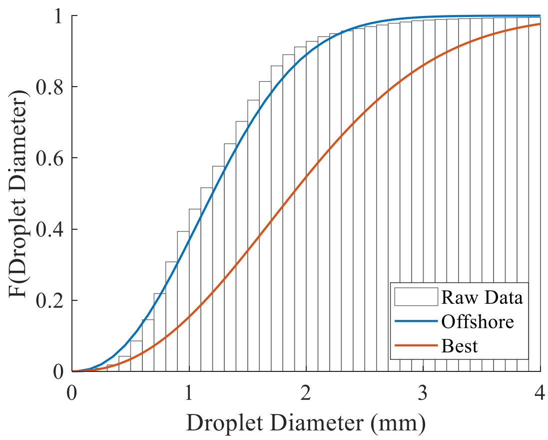

e) I = 10.0194 mm/hr

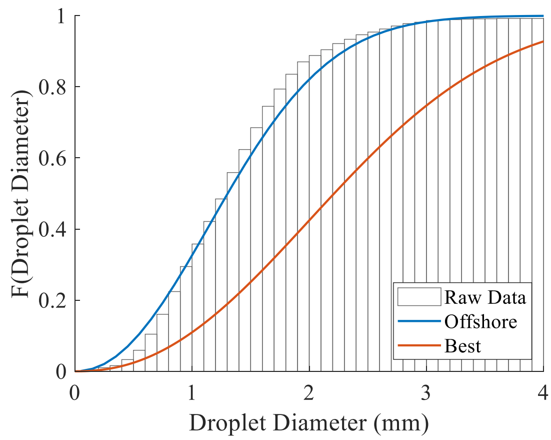

f) 19.9687 mm/hr

Figure 10: Comparison between the offshore DSD and the Best DSD at precipitation intensities a) 0.09998 mm/hr, b)0.9971, c) 2.5493, d) 5.0769, e) 9.9653 and f) 20.3311 mm/hr.

Fig 10. reveals that the Best DSD significantly overestimates the diameter of droplets. This is particularly true at the higher precipitation intensities. The goodness of fit of the offshore and Best DSD has been evaluated across the range of precipitation intensities in Fig. 11. The offshore DSD aligns well with the raw data and possesses a high coefficient of determination (R^2) across the precipitation intensity range. The slight reduction in R^2 at higher intensities can be attributed to the reduced amount of heavy and violent precipitation recorded. The coefficient of determination of the Best DSD reduces significantly as the precipitation intensity increases. Therefore, it is not appropriate to validate offshore weather radar data against the Best DSD.

https://doi.org/10.5194/wes-2020-11
Preprint. Discussion started: 12 February 2020

WIND ENERGY SCIENCE DISCUSSIONS

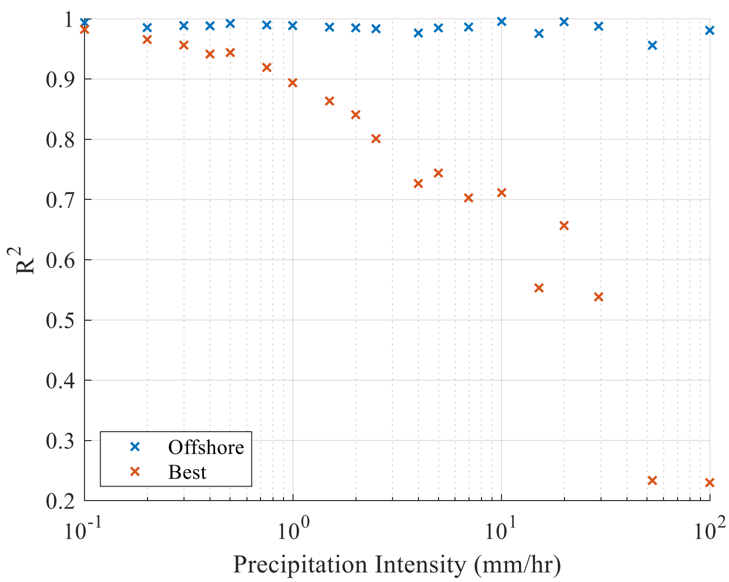

Figure 11: Coefficient of determination of the offshore DSD and the Best DSD across a range of precipitation intensities.

5.4 Limitations

The offshore DSD presented has two main limitations. Firstly, the presented measurement period may be a limiting factor. As the disdrometer continues to collect data, the DSD can be further refined. Secondly, data has only been collected at one point. Offshore DSDs may vary from location to location. To address this, a disdrometer has been positioned at ORE Catapult's Levenmouth offshore demonstration turbine for future comparison and validation.

6 Conclusions

DSDs are important in predicting and modelling leading edge erosion. Currently, there is a lack of an offshore dataset and the industry validates weather radars against onshore data. In this work, a disdrometer has been positioned three nautical miles offshore to collect and characterise the offshore precipitation environment and to provide an offshore dataset for validating weather radar predictions.

Heavy and violent precipitation was rare in the measurement period, accounting for less than 3.5 hours of precipitation across the year. Therefore, erosion damage is not likely to be driven exclusively by heavy and violent precipitation. Rain was the most frequently occurring hydrometeor, whereas snow, ice and hail particles were scarce. A clear distinction was visible in the diameter-velocity plots for each hydrometeor, with snow particles occurring across a wider range of diameters and lower average velocities. The majority of raindrops observed had a diameter below 2 mm.

https://doi.org/10.5194/wes-2020-11
Preprint. Discussion started: 12 February 2020

A general offshore DSD has been presented. The raw data was compared to the presented DSD and the most widely used DSD proposed by Best. The offshore DSD aligned well with the data. In contrast, the Best DSD significantly overestimated the diameters of droplets and is not a suitable validation for weather radars and use in lifetime prediction models.

The results presented address the lack of an offshore dataset and provide a general offshore DSD that can be used to validate weather radar predictions. A disdrometer has been placed at ORE Catapult's Levenmouth offshore wind turbine to provide further information about the precipitation environment and validate the presented DSD. The offshore dataset can be used to improve prediction and modelling techniques, reducing lost energy production and unexpected turbine downtime.

The aim of the industry is to develop a methodology that can predict the lifetime of a protection system on a wind turbine from rain erosion tests. The DNV-GL project COBRA aims to address this. The project uses the Best DSD to characterise the offshore environment. However, this DSD has been shown to be unsuitable for the offshore environment and any offshore lifetime prediction determined using it is unlikely to be accurate.

Data availability. Please contact the corresponding author.

Author contributions. RH had the lead on paper writing, data analysis and derived conclusions. KD and PH were responsible for installing and setting up the disdrometers. KD and CW supervised the research.

Competing interests. The authors declare that they have no conflict of interest.

Acknowledgments. This work was supported by the Engineering and Physical Sciences Research Council through the EPSRC Centre for Doctoral Training in Composites Manufacture (Grant: EP/K50323X/1), project partners the Offshore Renewable Energy Catapult <https://ore.catapult.org.uk>, and the EPSRC Future Composites Manufacturing Hub (grant: EP/P006701/1). The authors would also like to thank the Wind Blade Research Hub for their support in delivery of this manuscript. All data necessary to reproduce the results and support the conclusions are included within this paper.

References

Agnew, J.: Final report on the operation of a Campbell Scientific PWS100 present weather sensor at Chilbolton Observatory., 2013.

Bech, J. I., Hasager, C. B. and Bak, C.: Extending the life of wind turbine blade leading edges by reducing the tip speed during extreme precipitation events, Wind Energy Sci., 3(2), 729–748, doi:10.5194/wes-3-729-2018, 2018.

Best, A. C.: The size distribution of raindrops, Q. J. R. Meteorol. Soc., 76(327), 16–36, doi:10.1002/qj.49707632704, 1950.

Chen, B., Wang, J. and Gong, D.: Raindrop Size Distribution in a Midlatitude Continental Squall Line Measured by Thies Optical Disdrometers over East China, J. Appl. Meteorol. Climatol., 55(3), 621–634, doi:10.1175/JAMC-D-15-0127.1, 2016.

Doagou-Rad, S. and Mishnaevsky, L.: Rain erosion of wind turbine blades: computational analysis of parameters controlling the surface degradation, Meccanica, 0123456789, doi:10.1007/s11012-019-01089-x, 2019.

Eisenberg, D., Laustsen, S. and Stege, J.: Wind turbine blade coating leading edge rain erosion model: Development and validation, Wind Energy, 21(10), 942–951, doi:10.1002/we.2200, 2018.

Finans: Siemens sets billions : Ørsted must repair hundreds of turbines, windAction [online] Available from: http://www.windaction.org/posts/47883-siemens-sets-billions-orsted-must-repair-hundreds-of-turbines#.Xa2o8ehKiUk (Accessed 21 October 2019), 2018.

Kathiravelu, G., Lucke, T. and Nichols, P.: Rain Drop Measurement Techniques: A Review, Water, 8(1), 29, doi:10.3390/w8010029, 2016.

Keegan, M. H., Nash, D. H. and Stack, M. M.: Modelling Rain Drop Impact of Offshore Wind Turbine Blades, in ASME Turbo Expo 2012: Turbine Technical Conference and Exposition, pp. 887–898, American Society of Mechanical Engineers, Copenhagen, Denmark., 2012.

Met Office: Fact sheet No. 3 – Water in the atmosphere., 2007.

Slot, H. M., Gelinck, E. R. M., Rentrop, C. and van der Heide, E.: Leading edge erosion of coated wind turbine blades: Review of coating life models, Renew. Energy, 80, 837–848, doi:10.1016/j.renene.2015.02.036, 2015.

Sommerville, D. R. and Matta, J. E.: A method for determinging droplet size distributions and evaporational losses using paper impaction cards and dye trackers., 1990.

Springer, G. S., Yang, C.-I. and Larsen, P. S.: Analysis of Rain Erosion of Coated Materials, J. Compos. Mater., 8(3), 229–252, doi:10.1177/002199837400800302, 1974.

Vejen, F., Tilg, A., Nielsen, M. and Hasager, C.: D1.2 Precipitation statistics for selected wind farms., 2018.